Journal of Electronic Materials (2023) 52:7554–7565
https://doi.org/10.1007/s11664-023-10670-w

ORIGINAL RESEARCH ARTICLE

Ultrathin GaN Crystal Realized Through Nitrogen Substitution of Layered GaS

Jun Cao[1] · Tianshu Li[2] · Hongze Gao[1] · Xin Cong[3] · Miao-Ling Lin[3] · Nicholas Russo[4] · Weijun Luo[1] · Siyuan Ding[5] · Zifan Wang[1] · Kevin E. Smith[4] · Ping-Heng Tan[3] · Qiong Ma[5] · Xi Ling[1,2,6]

Received: 24 May 2023 / Accepted: 3 August 2023 / Published online: 2 September 2023

Abstract

GaN has been demonstrated as an important wide-bandgap semiconductor in many applications, especially in optoelectronic and high-power electronics. Two-dimensional (2D) GaN, with increased bandgap compared to the bulk counterpart, not only amplifies existing functionalities but also opens up fresh possibilities for compact electronics. Although several methods have recently been developed to synthesize 2D GaN, their practical application is hampered by either harsh growth conditions (e.g., high temperature and ultrahigh vacuum) or unsatisfactory performance due to grain boundaries. Here, we report the realization of few-nanometer-thick GaN crystals via in situ atomic substitution of layered GaS flakes at a relatively low temperature (590°C). GaN with tunable thickness from 50 nm down to 0.9 nm (~2 atomic layers) is achieved by applying the atomic substitution reaction to GaS with different numbers of layers. The obtained ultrathin GaN flakes retain the morphology inherited from the GaS flakes and show high crystallinity by transmission electron microscopy (TEM) characterization, while the thickness of GaN decreases to about 72% of the corresponding GaS flakes from the atomic force microscopy characterization. A time-dependent mechanism study reveals both horizontal and vertical conversion paths, with Ga_2S_3 as intermediate. Photoluminescence (PL) spectroscopy measurements show that the band edge PL of 2D ultrathin GaN is blue-shifted as compared with bulk GaN, suggesting that the bandgap increases with the decrease in thickness. This study provides a promising method for obtaining ultrathin, high-crystallinity GaN with tunable thicknesses, utilizing a minimal thermal budget. This breakthrough lays a solid foundation for future investigations into fundamental physics and potential device applications.

Keywords Atomic substitution · 2D GaN · ultrathin · wide bandgap · semiconductor

Introduction

Two-dimensional (2D) materials serve as an exceptional platform for groundbreaking applications, owing to the unprecedented physics observable at the nanoscale.[1–4] Among these, van der Waals (vdW) materials are studied extensively, primarily due to the abundant access to high-quality 2D crystals.[5–12] Compared with conventional vdW 2D materials, less study has been devoted to non-vdW group III–V 2D semiconductors. It was not until recently that atomically thin 2D crystals of a few three-dimensional binary compounds (e.g., GaN) were synthesized, which significantly broadens the range of multifunctional 2D materials.[13–19] When present in 2D forms where quantum confinement effects are manifested, dramatically different electronic properties from their bulk counterparts are observed.[15,20–22] For instance, the bandgap of 2D GaN is predicted to be

✉ Xi Ling
xiling@bu.edu

1 Department of Chemistry, Boston University, 590 Commonwealth Avenue, Boston, MA 02215, USA

2 Division of Materials Science and Engineering, Boston University, 15 St. Mary's Street, Boston, MA 02215, USA

3 State Key Laboratory of Superlattices and Microstructures, Institute of Semiconductors, Chinese Academy of Sciences, Beijing 100083, People's Republic of China

4 Department of Physics, Boston University, 590 Commonwealth Avenue, Boston, MA 02215, USA

5 Department of Physics, Boston College, Chestnut Hill, MA 02467, USA

6 The Photonics Center, Boston University, 8 St. Mary's Street, Boston, MA 02215, USA

blueshifted to 5.28 eV compared with that of bulk GaN ($E_g = 3.4$ eV),[23] which is also observed experimentally in ultrathin GaN prepared from migration-enhanced encapsulated growth (MEEG) utilizing epitaxial graphene.[15] Benefiting from the wide bandgap and high electron mobility (2000 $cm^2/V/s$) of GaN, two-dimensional electron gas in a GaN-based heterostructure has long been utilized for high-power and high-frequency optoelectronic devices.[24–27] In addition, GaN has demonstrated excellent performance in fabricating efficient blue and deep UV light-emitting diodes due to their wide bandgap. 2D GaN is of particular interest because the extreme quantum confinement effect offers additional tuning of the light-emitting properties.[28] Meanwhile, the ultrathin nature would bring mechanical flexibility to the devices and also open opportunities to integrate with existing 2D materials for unprecedented properties and applications. To this end, developing synthesis strategies for ultrathin GaN with high crystallinity, satisfactory area and controlled thickness is highly desired.

Epitaxial growth in molecular beam epitaxy (MBE)[29–32] and chemical vapor deposition (CVD)[33,34] processes are commonly utilized to produce large-area GaN films for industrial optoelectronic applications. The ideal substrate with minimum lattice mismatch for MBE synthesis is the GaN bulk crystals, which remain challenging and expensive to obtain.[35,36] Moreover, thin films created via MBE or metal–organic chemical vapor deposition (MOCVD) often present as small islands, fused together with abundant grain boundaries. These may influence the electrical properties of devices based on GaN. To harness GaN's full potential, there is a high demand for innovative technologies capable of producing superior quality GaN.[35,36] Besides conventional synthesis approaches, novel methods have recently been developed to prepare 2D GaN. Robinson and co-workers synthesized 2D GaN using a migration-enhanced encapsulation growth technique with epitaxial graphene.[15] However, the nanometer-size flakes pose a tremendous challenge for fabricating electronic devices on such 2D GaN, where poor mobility can greatly limit their practical applications.[37,38] Several other approaches utilizing surface-confined nitriding reaction strategies have been developed to synthesize ultrathin GaN with relatively large area. For instance, Daeneke and co-workers transferred ultrathin Ga_2O_3 films formed on the surface of liquid Ga droplets onto a substrate and further converted it into ultrathin GaN film through a nitriding reaction.[17] Although the as-prepared ultrathin GaN features large lateral dimensions up to several centimeters, the samples suffer from short-range crystallinity, which creates a bottleneck for achieving high-performance electronics. To the best of our knowledge, for the reported methods, either the synthesis requires high temperatures above 800°C (e.g., in liquid metal and graphene encapsulation methods), or the produced GaN films consist of small islands connected by a significant number of grain boundaries (e.g., in MBE and MOCVD techniques). These factors may adversely affect the electron mobility in the material.[39–43]

Inspired by the atomic substitution approach we developed recently for ultrathin non-vdW materials,[19] we use vdW layered GaS as precursors for ultrathin non-vdW GaN through a nitriding reaction. In this process, the morphology of GaN is inherited from GaS flakes, and the thickness of GaN decreases to 72% of the corresponding thickness of GaS. We observe both horizontal and vertical conversion paths which are more obvious in relatively thick flakes with Ga_2S_3 as an intermediate. More importantly, the obtained ultrathin GaN flakes are found to be highly crystalline, owing to the small lattice mismatch between GaS (3.587 Å)[44] and GaN[18] (3.323 Å). When compared to the bulk GaN, a significant blue shift in the band edge photoluminescence (from 3.5 eV to 3.7 eV) is discernible in the ultrathin GaN produced, indicating a wider bandgap for this material. Leveraging the benefits of our methodology, our research paves the way for expanded exploration of the science and applications related to ultrathin GaN.

Results and Discussion

Synthesis of Ultrathin GaN and Structural Characterization

Through atomic substitution of sulfur in GaS flakes with nitrogen, we obtain ultrathin 2D GaN crystals, which conventionally are challenging to access because of their non-layered structures (Fig. 1a). The conversion process was performed in a tube furnace (Fig. S1) at 590°C through a gas–solid reaction between ammonia gas and GaS flakes. The ammonia gas is generated by purging Ar gas through ammonium hydroxide solution (~30%), after which the ammonia gas is carried by 200 sccm Ar gas through a dryer filled with KOH and CaO powers, where most of the moisture can be removed. Optical images of the flakes taken before and after the reaction show that the flakes retained their original morphology, while the optical contrast changed (Fig. 1b and c), reflecting distinct absorption properties of the two materials.[32,45] After conversion, the flake depicted in Fig. 1c is characterized by atomic force microscopy (AFM) measurements (Fig. 1d), revealing a 1.4-nm GaN flake with smooth surface, as further substantiated by the height profile provided in Fig. 1e. Raman spectroscopy measurements show the typical Raman features from GaS disappear after the reaction (Fig. S2), indicating that the flakes have been converted into a different material, which is later confirmed to be GaN.

We attribute the successful synthesis of high-crystallinity ultrathin GaN to the smaller lattice mismatch with the

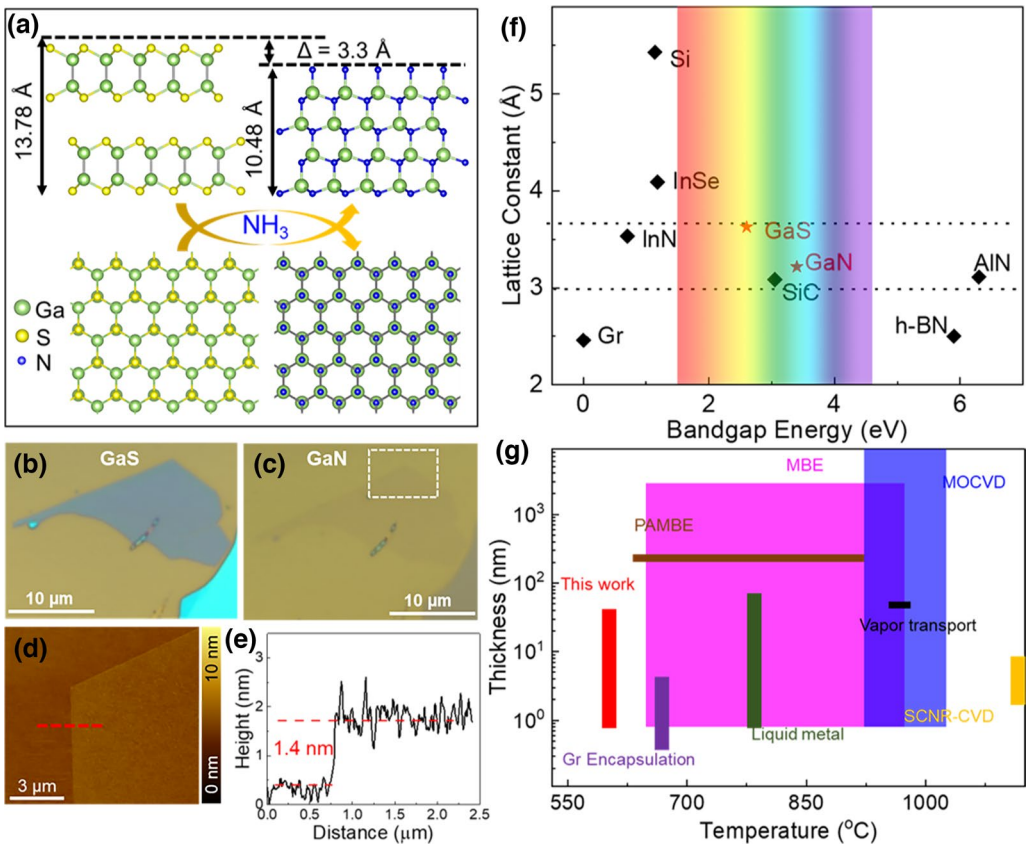

Fig. 1 (a) Structure illustration of GaS and GaN. (b) Optical image of GaS. (c) Optical image of GaN converted from GaS in (b). (d) AFM image of the area highlighted by a white rectangle in (c). (e) AFM height profile measured along the red dashed line in (d). The thickness extracted from AFM is 1.4 nm. (f) Diagram of in-plane lattice parameter versus bandgap energy, establishing the possibility of probing deep into the ultraviolet regime with access to ultrathin 2D GaN. GaS and GaN in this work are highlighted with red stars. The dashed lines are to illustrate the potential substrates with lattice mismatch in the range of −4% to 12.7% from GaN. Si as the commonly used substrate is out of range which does not work well with the synthesis of GaN. (g) Comparison of processing temperature and accessible thickness of GaN prepared through different approaches: Gr encapsulation: migration-enhanced encapsulated growth (MEEG) technique utilizing epitaxial graphene;[15] liquid metal: ammonolysis of liquid metal derived 2D oxide sheets;[17] PAMBE: plasma-assisted molecular beam epitaxy;[46,47] MOCVD: metalorganic chemical vapor deposition;[48–53] MBE: molecular beam epitaxy;[29–32,54–58] vapor transport: infrared close space vapor transport;[59] SCNR-CVD: surface-confined nitriding reaction via chemical vapor deposition.[18] Data taken from Refs. 15, 17, 18, 29–32, 46, 47, 48–53, 54–58, and 59 (Color figure online).

GaS crystal precursor (see Fig. 1f), as opposed to conventional substrates such as sapphire or Si. Despite the contrast between the layered structure of GaS and the non-layered structure of GaN, the Ga atoms in both configurations display a hexagonal lattice. Furthermore, the lattice mismatch of GaS (3.627 Å) and GaN (3.216 Å)[18,44] is about 12.7%, a value comparable to the 15% lattice mismatch between GaN and sapphire (2.747 Å), which is a frequently utilized substrate for the epitaxial growth of GaN.[60] Consequently, high-crystalline ultrathin GaN crystals are realized through the nitrogen substitution of layered GaS. In contrast, the Si substrate exhibits a considerably larger lattice constant (5.431 Å), which often makes the direct deposition of high-quality 2D GaN film challenging, yielding samples of inferior quality with a high density of dislocations. Few successful attempts at the growth of GaN film on an Si substrate have been achieved, but these typically require the sacrifice of a buffer layer ranging from 300 Å to 900 Å.[61,62] Considering that a 12.7% lattice mismatch is still significant, an extensive amount of tension during the growth is anticipated. An additional advantage of our atomic substitution method, when compared to traditional epitaxial growth, lies in its ability to effectively dissipate the strain caused by the lattice mismatch between GaS and GaN, owing the van der Waals gaps present within the GaS layers. As a result, structural cracking during the reaction is averted due to the combined effect of the "relatively small" mismatch and the efficient dissipation of strain. Therefore, the resulting ultrathin GaN flakes maintain the morphology and continuity of the original GaS flakes.

When contrasted with existing methodologies for synthesizing 2D or ultrathin GaN, our approach stands out due to

its significant advantages, including the utilization of low-temperature processes (compared with MOCVD and liquid metal methods) and the provision of a wide array of thicknesses ranging from a few nanometers to tens of nanometers without sacrificing the grain sizes (Fig. 1g). In Fig. S3, we have shown some examples of AFM images of GaN of various thicknesses together with their corresponding optical images. The low-temperature process not only saves the thermal budget in manufacturing, but also offers an opportunity to integrate GaN with other platforms through monolithic 3D integration technology without damaging existing structures on it, which has been demonstrated to be an advanced technology for large-scale circuits fabrication recently.[39–43] The effortless control over varying thicknesses of GaN paves the way to investigate the fundamental physical properties of GaN within the quantum confinement regime. This further provides an opportunity to uncover new functionalities for advanced electronic devices. Moreover, as it is potentially convenient to obtain large-area vdW GaS crystals using conventional 2D material preparation methods (e.g., wafer scale CVD synthesis),[44] we anticipate our approach could lead to the achievement of large-area ultrathin GaN film, allowing further engineering for practical applications.

To gain insights into the atomic structure of the synthesized GaN, high-resolution transmission electron microscopy (HRTEM) measurements are performed by transferring GaS flakes directly onto a Si_3N_4 TEM grid for the conversion reaction followed by HRTEM characterization. Similar to GaN prepared on a SiO_2/Si substrate, the morphology of flakes is retained while distinct optical contrast is observed after conversion (Fig. S4). Figure 2a shows a typical low-magnification TEM image of a GaN flake, showing the smooth surface of the whole flake. A zoomed-in HRTEM image (Fig. 2b) of the area highlighted with a yellow square in Fig. 2a clearly displays the crystalline structure of GaN and a distance of 0.29 nm between two adjacent lattice planes matching well with the distance between (100) planes in wurtzite GaN.[18] Compared with bulk GaN (0.279 nm), the distance between the (100) planes of our ultrathin GaN is about 4% larger, which is attributed to the strain induced in the lattice during the structure transformation.[20,21,63] When GaN is thinned down to the region where the surface plays an important role in stabilizing the structure, they tend to expand in the lateral direction in order to remove the destabilizing dipole.[22,63] Specifically, ultrathin films of GaN usually have a polar surface, leading to the divergence of the surface energy that makes the surface intrinsically unstable. To stabilize the polar surfaces, wurtzite structures commonly adopt a structural relaxation process where the geometry of surface atoms is altered away from sp^3 orbital hybridization towards a sp^2 trigonal planar geometry as the bond lengths reduce and the angles increase. The selected area electron diffraction (SAED) pattern shows a hexagonal lattice of the crystal over the entire flake, further confirming the wurtzite structure of the obtained GaN (Fig. 2c). Importantly, SAED patterns taken at four different locations on the flake show identical orientation, suggesting single crystallinity across the whole flake (Fig. 2c). In addition to the main hexagonal SAED pattern, other diffraction peaks were observed with varying brightness depending on the thickness of the flake, which corresponds well with the SAED simulation results (Fig. S5). Energy-dispersive spectroscopy (EDS) is further performed on a relatively thick GaN flake under SEM mode where N and Ga signal was observed and no S signal remains, indicating a complete conversion from GaS to GaN. Raman mapping is conducted to verify the uniform and complete conversion from GaS to GaN. Before conversion, Raman map of GaS shows uniform intensity distribution of A^1_{1g} peak (Fig. S6a), while no A^1_{1g} signal is observed after complete conversion (Fig. S6b). Figure 2d shows a SEM image of a GaN flake with a smooth surface, and its EDS elemental maps of Ga (Fig. 2e) and N (Fig. 2f) reveal uniform distribution of elements in the flake, suggesting great sample quality prepared by the atomic substitution method.

Investigation of the Conversion Mechanism

Upon substituting S in GaS with N, the vdW gaps are removed as N forms covalent bonds which connect the Ga atoms between two adjacent layers. In theory, the height of four layers of Ga (one unit cell in GaS) drops from 13.786 Å to 10.48 Å (two unit cells in GaN) according to the crystal structure of GaS and GaN (Fig. 1a). Therefore, we expect a decrease in thickness by about 24% when GaS is converted to GaN. To validate this hypothesis, we perform AFM to measure the thickness of flakes before and after conversion. Indeed, we observe that the thickness of GaN decreases compared with that of corresponding GaS. Figure 3a and b show an example of thickness change characterized by AFM, where two GaS flakes with thickness of 32 nm and 22 nm (Fig. 3c) are converted to GaN flakes with thickness of 23 nm and 15 nm (Fig. 3d), respectively. Additionally, by plotting the thickness of GaS with respect to GaN ranging from a few nanometers to ~80 nm (Fig. 3e), a linear correlation is established between the thickness of GaS before conversion and GaN after conversion. Pearson correlation analysis in Fig. S7 proves that the experimental and theoretical thickness difference are strongly correlated ($r = 0.87$). Ratios of GaN/GaS are plotted, yielding a horizontal trend line at 72%, suggesting a thickness decrease of 28% after conversion, which aligns well with the theoretical predication of 24%. The small deviation (~4%) from the theoretical value may originate from the uncertain gaps between flakes and the SiO_2/Si substrate, which may be especially predominant for thin flakes. When comparing the difference in experimental thickness (y_1) between GaS and GaN with

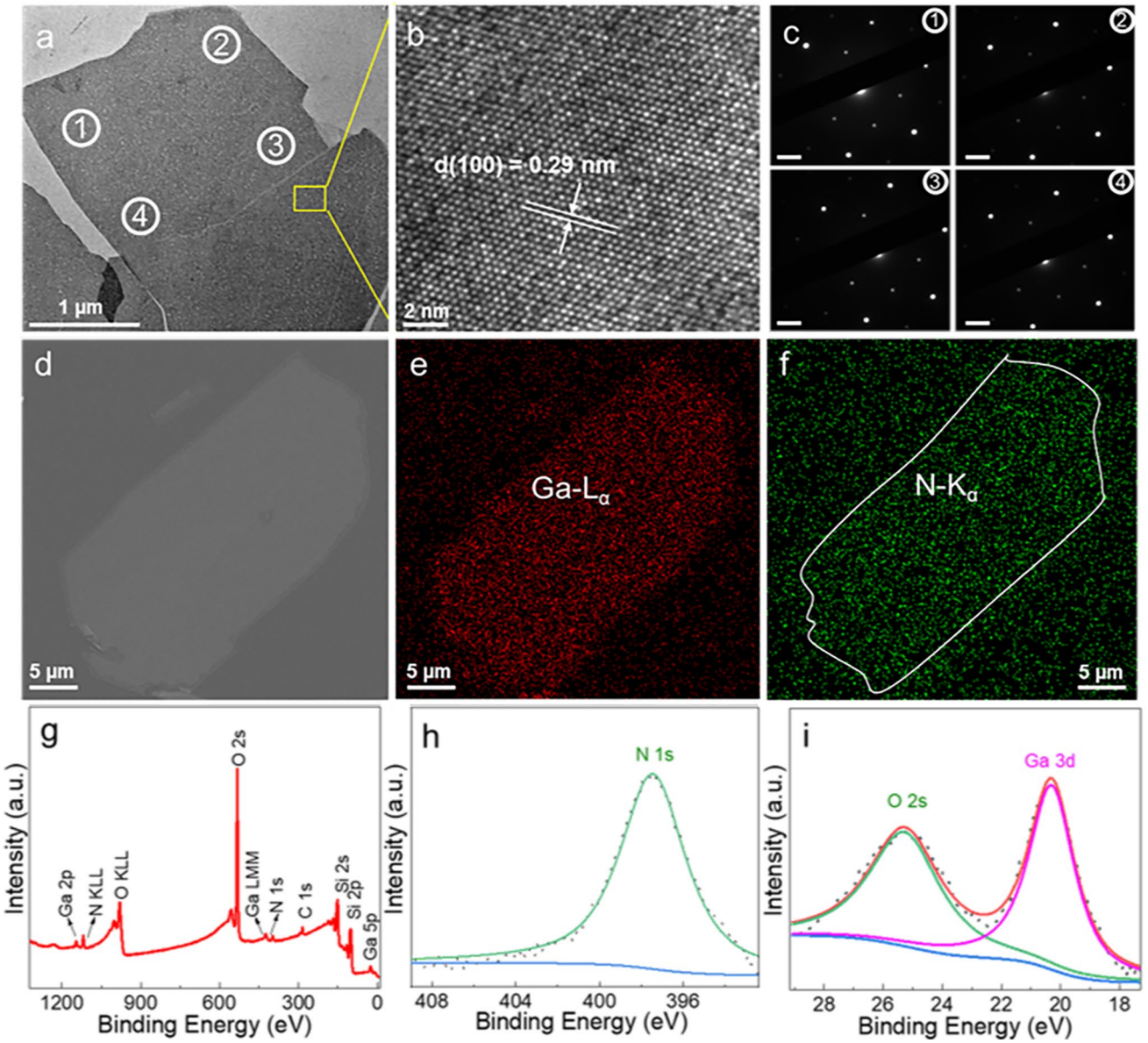

Fig. 2 Crystal structure and elemental analysis of GaN converted from GaS. (a) Low-magnification TEM image of GaN. (b) HRTEM image taken on the area indicated by yellow square in (a). (c) SAED patterns of an as-prepared GaN flake measured at different locations as indicated by white circles in (a). Scale bar: 5 1/nm. (d) SEM image of a GaN flake. (e, f) EDS elemental maps of Ga-Lα (e) and N-Kα (f) elements in the flake shown in (d). White line in (f) depicts the contour of the GaN flake shown in (d). (g) XPS survey scan of GaN; (h, i) XPS fine spectra of N 1s (h) and Ga 3d (i) core level peaks of GaN. O 2s is present due to the SiO_2/Si substrate. Spectra fitting lines and baselines (in blue) are shown in (h) and (i) (Color figure online).

the theoretical values (y_2) (Fig. 3f), we observe good agreement as shown by the small deviation between y_1 and y_2, which is also excellently demonstrated by the ratio of y_1/y_2 being close to 1. This trend persists for both thin and thick flakes encompassing various numbers of layers, given that a uniform conversion method is adhered to during the transformation process.

In order to unravel the conversion mechanism, we scrutinized the evolutionary changes in the structure throughout the conversion process. This was achieved by conducting thorough characterizations of the flake at various stages of the reaction. The multistep conversion is conducted at lower reaction temperature (~580°C) on a relatively thick flake (~35 nm) in the pursuit of better visualization. Following each step, we take the sample out and take optical images of the exact same flake. As shown from Fig. 4a, b, c, d, e and f, the converted area (darker contrast) labeled by white arrows expands with time accompanied by diminishment

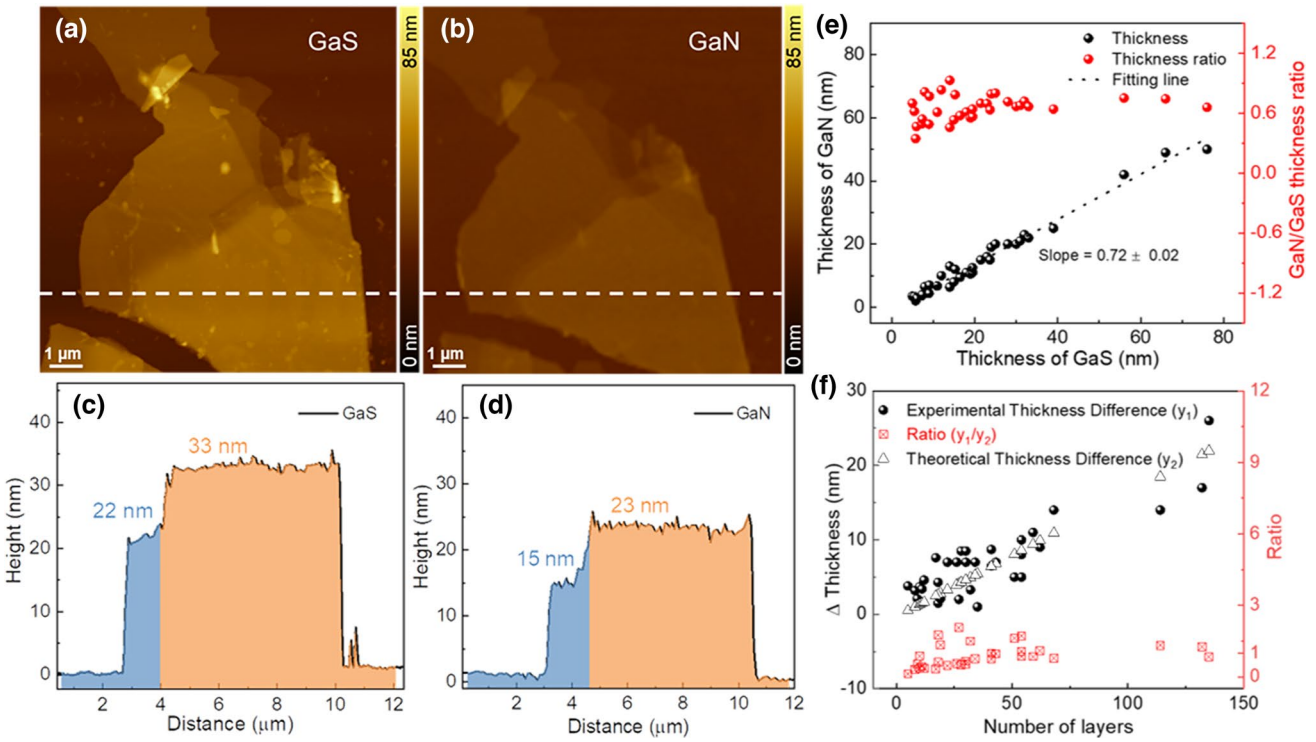

Fig. 3 AFM images of (a) GaS before conversion and (b) GaN after conversion. AFM height profiles extracted from (c) GaS and (d) GaN flake along the white dashed lines shown in (a) and (b), respectively. (e) Correlation plot of the thickness of GaS and converted GaN (in black). Data points in red show the corresponding thickness ratios of GaN/GaS. (f) Layer-dependent thickness study of the conversion from GaS to corresponding GaN. The number of layers is calculated through the thickness of GaS. Theoretical thickness difference $y_2 = N \times (d_{GaS} - d_{GaN})$, where N is the number of layers of GaS, d_{GaS} is the theoretical thickness of single-layer GaS, and d_{GaN} is the theoretical thickness of single-layer GaN. Experimental thickness difference y_1 = Experimental thickness of GaS − Experimental thickness of corresponding GaN (converted from the same GaS) (Color figure online).

of the unconverted area (brighter contrast), suggesting the progressive conversion from GaS to GaN via Ga_2S_3 intermediate. As an example, the optical contrast of the whole flake after reaction for 1 h (Fig. 4b) is drastically distinct from the original GaS flake (Fig. 4a), where the majority area (darker contrast) remains Ga_2S_3, as confirmed by Raman spectra, where both A_{1g} and F_{2g} vibrational modes from Ga_2S_3 are observed (Fig. 4g).[64] TEM images of both the unconverted and converted areas present distinct electron diffraction patterns from Ga_2S_3 and GaN, thereby corroborating our observations (as depicted in Fig. S8). The converted region of the thicker flake exhibits a darker contrast, and its Raman spectrum aligns with that of GaN. After a duration of 4.5 h, the entire flake is thoroughly converted, as evidenced by the uniform optical contrast across it. It is also worth mentioning that the reaction rate will increase significantly at elevated temperature (e.g. 590°C), and full conversion can be realized in a shorter period of time (~1 h). Nevertheless, when the reaction temperature is further increased, such as to 600°C, the appearance of cracks becomes more prevalent, a phenomenon possibly caused by the enhanced substitution rate at this higher temperature, as illustrated in Fig. S9.

Comparing reaction for 1 h at different temperatures further confirms the strong temperature dependence of the conversion from GaS to GaN. The Kelvin probe force microscopy (KPFM) measurements corroborate our observation with morphology and surface potential information. Although the AFM height image shows that the surface is very uniform over the whole flake, with a roughness of 1.5 nm in an intermediate state of the conversion (Fig. 4h), the surface potential varies drastically after the conversion. Figure 4i and j show the KPFM work function and surface potential image of the flake after 1.5 h conversion, showing distinct work functions between converted areas (GaN) and unconverted areas (Ga_2S_3), matching well with the observation from optical images. The area with a greater degree of conversion (iii in Fig. S10) shows higher surface potential as opposed to area with a lower degree of conversion (i, ii in Fig. S10). We evaluate the morphology by extracting the surface root mean square (RMS) roughness of the flake and plotting it over reaction time, where negligible roughness change is observed (Fig. 4k). Additionally, we have charted the percentage conversion from Ga_2S_3 to GaN based on the area of each compound depicted in the optical images from Fig. 4a,

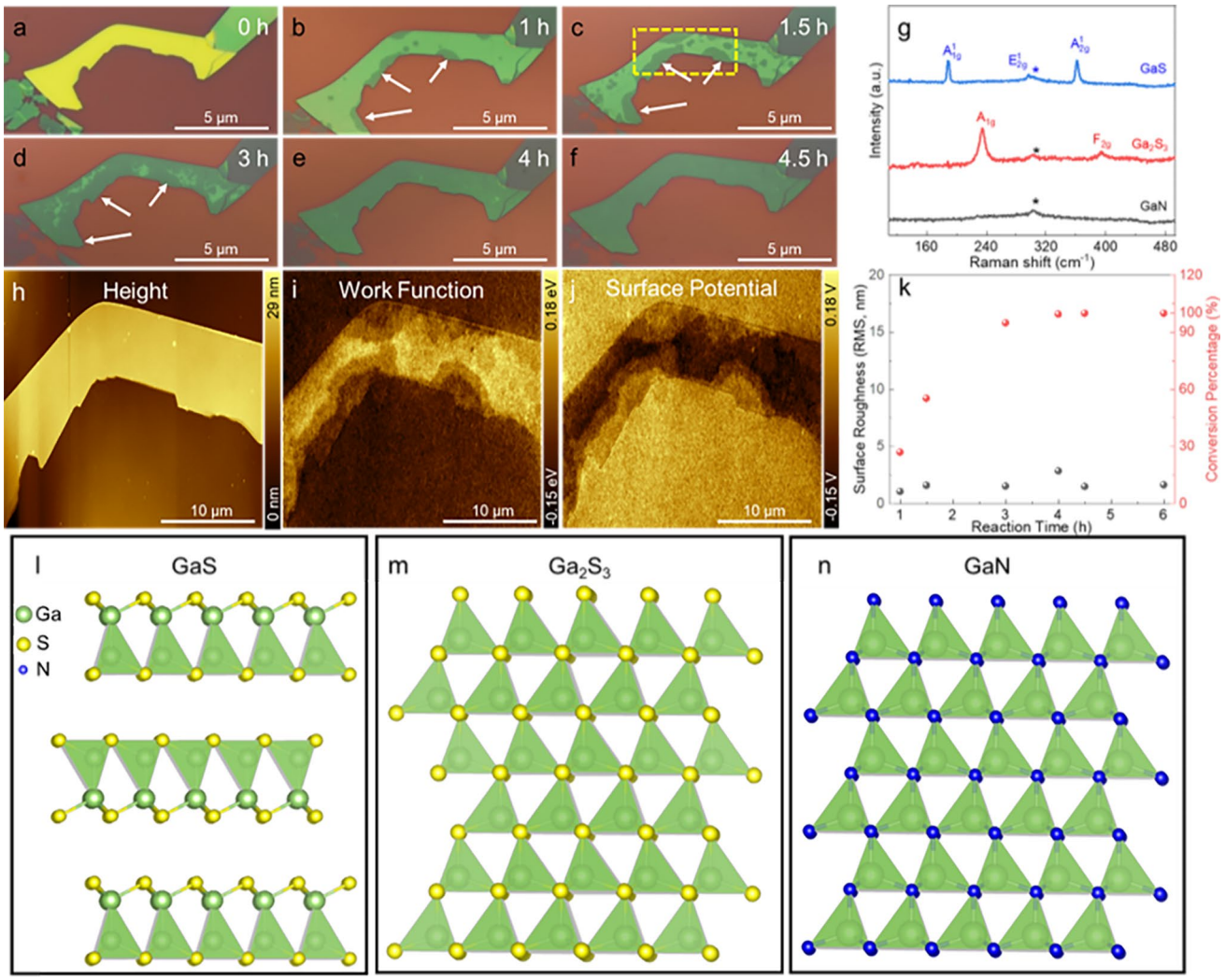

Fig. 4 Study of the mechanism of conversion from GaS to GaN. (a–f) Roadmap of optical images taken at different stages of the conversion process from GaS to GaN with Ga_2S_3 as intermediate. The white arrows indicate the areas with darker contrast that are converted from Ga_2S_3 to GaN. (g) Raman spectra of GaS, Ga_2S_3 and GaN. The peaks labeled with an asterisk (*) are from the SiO_2/Si substrate. (h–j) Height (h), work function (i) and surface potential (h) images obtained from KPFM measurements of the area highlighted with the yellow rectangle in (c). (k) Conversion percentage plot of GaS to GaN at various stages (in red) and surface roughness study (in black). The conversion percentage is calculated by comparing the area with darker contrast shown in optical images at different conversion time over the area of the whole flake. Surface roughness is extracted from height profile of the same area of various conversion stages as highlighted in yellow rectangle shown in (c); (l–n) Polyhedral structure illustration of GaS (l), Ga_2S_3 (m) and GaN (n), respectively (Color figure online).

b, c, d, e and f. In the first 3 h, the converted area expands rapidly relative to the reaction time, whereas the subsequent 1.5 h reveals only a minimal change in the converted area as the conversion nears 100%. We attribute the Ga_2S_3 intermediate to the lower standard Gibbs free energy of formation of Ga_2S_3 around the conversion temperature (~580°C).[65] Despite the absence of an external S source, nucleation of Ga_2S_3 can still be realized by enrichment of S locally from GaS (Fig. 4l), which is more thermodynamically favorable. Eventually, with the flow of NH_3, S is carried out and Ga_2S_3 (Fig. 4m) will gradually be converted to GaN (Fig. 4n) when high-vapor-pressure NH_3 takes over. It is worth mentioning here that the size of the NH_3 molecule (3.26 Å) is smaller than the gap between GaS layers (4.07 Å), which allows for free diffusion, enabling the conversion of the interior and exterior area of GaS (Fig. S11).

Moreover, we have noted varying reaction dynamics between thin and thick flakes. Based on optical images, thin flakes undergo conversion to GaN within 1 h at 580°C, whereas thicker flakes require a longer duration to achieve full conversion, as demonstrated by the non-uniform optical contrasts at different areas of the flake

(see Fig. S9a and b). The progression of the converted area over time, coupled with the rate discrepancy between thin and thick flakes, suggests that the conversion process might proceed in two directions: both horizontally and vertically. Horizontally, the converted area is initiated from the edge area where defects and dangling bonds are present in higher abundance, then gradually expands from the edge to the central area of the flake. Vertically, thin flakes with a smaller number of layers finishes conversion within shorter time compared with thick flakes. Both GaS and Ga_2S_3 coexist in the converted area of thick flakes, implying that the reaction starts from the top surface inward to the bottom. Hence, when the reaction is incomplete, the top part of the flake is Ga_2S_3 and GaN, while the bottom part remains GaS. It is reasonable to believe that vertical reaction is the rate-limiting step, as thinner flakes convert within a shorter period of time where no vertical heterostructure is observed. The low-magnification TEM image in Fig. S12a shows a thin flake of GaN with a smooth surface. SAED of the area (Fig. S12b) confirms the highly crystalline nature of GaN with only one diffraction pattern set. We utilize x-ray photoelectron spectroscopy (XPS) to investigate the chemical composition and oxidation states of the GaN samples. The survey scan spectrum from the XPS analysis in Fig. 2g reveals the presence of Ga, N from GaN sample and C, O, Si which are either from the SiO_2/Si substrate or from the environment. The broad N 1s peak centered at ~397.6 eV corresponds to the binding energy of N in GaN.[15,17,66] In Ga 3d region, both Ga 3d and O 2s (from SiO_2/Si) are observed since their binding energies are close.[17] It is worth mentioning here that no residual S peaks associated with GaS are observed (Fig. S13),[64] which is expected for the full conversion from GaS to GaN.

Enlarged Bandgap of 2D GaN Revealed by PL Study

To determine the optical bandgaps of the obtained ultrathin GaN with various thicknesses, we further measured the PL emission spectra using 266 nm laser excitation. As shown in Fig. 5a, pronounced PL signals were observed from samples from 25 nm down to 4.4 nm. Importantly, the emission energy is blue-shifted from 3.5 eV for the 25 nm thick sample to 3.7 eV for the 4.4-nm-thick sample with the decrease in sample thickness, suggesting an increase in the optical bandgap of GaN. The results match well with the theoretical prediction of the increase in the bandgap of 2D GaN.[15] Note that a 5.28 eV bandgap was predicted for a single-layer GaN in the literature,[15] but we did not observe PL signals from thinner samples, probably due to weak signals. We plot the bandgap against the thickness of six samples in Fig. 5b, where an evident blue shift with decreasing thickness exhibits a signature quantum confinement effect in the 2D limit. By using GaS precursors of different thicknesses, we successfully engineered optical bandgaps of GaN flakes of various thicknesses using our atomic substitution approach. In addition, we observed typical red defect emission at around 620 nm from the obtained GaN (Fig. S14), which has been widely reported in GaN synthesized using many other methods as the C and O doping-induced defect emission.[54,59,67]

The thickness-dependent PL can be understood more quantitatively by examining the excitonic peak position with an intuitive model that involves quantum confinement and exciton binding energy as well as Bohr radius. To extract the Bohr radius, we plot the PL peak position of exciton E_c of the as-prepared GaN flakes with varying thickness. We find that flakes with thickness larger than 11 nm have a linear dependence on $1/L^2$, which can be fitted by the conventional model of infinite quantum wells as:[68,69]

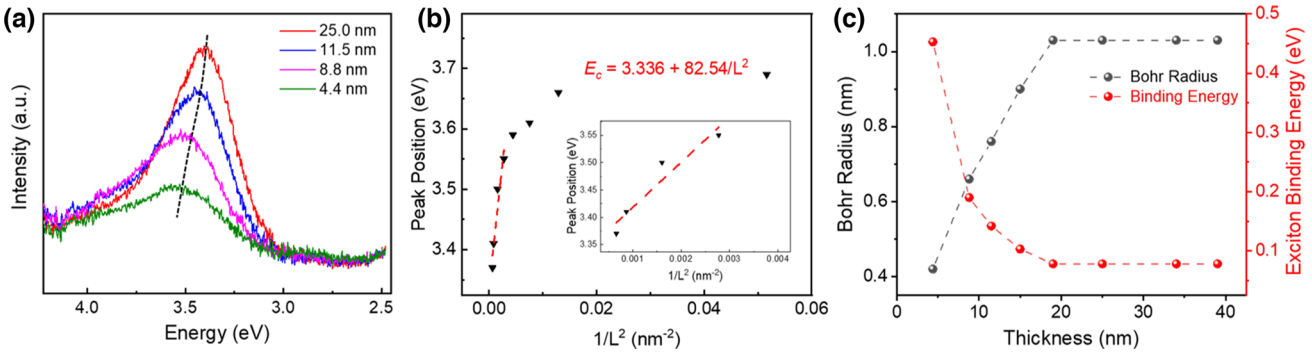

Fig. 5 Thickness-dependent PL of GaN. (a) PL spectra of four GaN samples with different thicknesses. (b) Layer-dependent excitonic effect in as-prepared GaN flakes. The position of the PL peak in GaN as a function of $1/L^2$, where L is the thickness of the film. The red line is the fitting result using the model of infinite quantum well with the fitting equation given as shown. The inset is a magnified version of the area indicated by the dashed red rectangle. (c) The dependence of the binding energy and exciton radius in GaN flakes on the sample thickness (Color figure online).

$$E_c = E_g + R_y + \frac{\Pi^2\hbar^2}{2mL^2} - R_y \quad (1)$$

where L is thickness of the GaN flake, E_c is the exciton peak position, E_g is the excitonic resonance energy in bulk GaN, R_y is the exciton binding energy and assumed to be unchanging with the thickness in the model of infinite quantum wells, and m is the reduced electron–-hole effective mass of the flake. The fitting to the experimental results yields:

$$E_c = 3.336\ \text{eV} + \frac{82.54}{L^2} \quad (2)$$

from which we can derive the reduced effective mass $m = 0.457\ m_0$ for the exciton in GaN flakes that are thicker than 19 nm. Based on the fitting results, we can also derive the exciton binding energy $R_y = 78$ meV and the Bohr radius $a = 1.03$ nm, which is in the same order of reported Bohr exciton radius (2.5 nm) for GaN,[70–72] in which the static dielectric constant is set to be 8.9 as previously measured for bulk GaN.[70,73]

The peak position of exciton E_c of GaN flakes thinner than 19 nm shows apparent deviation from the model of infinite quantum wells. Instead, we can fit the experimental results with a model of quantum wells with fractional-dimensional space as:

$$E_C = E_g + R_y + \frac{\Pi^2\hbar^2}{2mL^2}\left[(D-1)/2\right]^2 - \frac{R_y}{\left[(D-1)/2\right]^2} \quad (3)$$

where D is the effective dimensionality defined by the ratio of the exciton binding energy in the GaN flakes (R_y*) and that of bulk GaN (R_y) as:

$$\left[(D-1)/2\right]^2 = R_y/R_y^* \quad (4)$$

The factor of $\left[(D-1)/2\right]^2$ originates from the change in the effective mass associated with the effective dimensionality. For the flakes thicker than 11 nm, D is 3 and Eq. 4 is reduced to the equation for infinite quantum wells. By fitting the experimental results with Eq. 4, we obtain effective dimensionality D of 1.83, 2.28, 2.48, 2.74 for GaN flakes with thickness of 4.4 nm, 8.8 nm, 11.5 nm, 19 nm, respectively. We then derive the corresponding exciton binding energies using Eq. 4 to be 0.453 eV, 0.19 eV, 0.142 eV and 0.103 eV for the corresponding GaN flakes; we also derive the corresponding Bohr radius of excitons from $a_b^* = a_b(D-1)/2$ as 0.42 nm, 0.66 nm, 0.76 nm and 0.90 nm, respectively. The variation in the Bohr radius and exciton binding energies suggest that the thickness of the GaN can be utilized as an important knob to tune the optical and electronic properties of GaN.

Conclusion

In conclusion, we have successfully fabricated ultrathin GaN nanosheets through the process of nitrogen substitution in GaS at a moderately low temperature of approximately 590°C. By capitalizing on the readily accessible van der Waals (vdW) layered structure of GaS precursors with a range of thicknesses, we have devised a straightforward method to create high-quality, ultrathin 2D GaN. This method further allows for thickness tuning down to sub-nanometer levels. Through our exploration of the time-dependent conversion process, we have unveiled a conversion mechanism from GaS to GaN that involves Ga_2S_3 as an intermediary stage. The optical bandgap of our ultrathin GaN was identified through photoluminescence (PL) measurements, revealing an enlarged bandgap in comparison to the bulk form. A thickness-dependent quantum confinement effect was also studied through examination of the Bohr radius and exciton binding energy. We believe that the benefits of our atomic substitution strategy could present extensive opportunities to delve into both the fundamental science behind ultrathin GaN, and its potential applications in device technology.

Supplementary Information The online version contains supplementary material available at https://doi.org/10.1007/s11664-023-10670-w.

Acknowledgments This research is primarily supported by the U.S. Department of Energy (DOE), Office of Science, Basic Energy Sciences (BES), under Award DE-SC0021064. X.L. and J.C. also acknowledge the support of Semiconductor Research Cooperation (SRC) under Award S4994. Work by W.J.L. and X.L. was supported by the National Science Foundation (NSF) under Grant No. (1945364). X.L. acknowledges the membership of the Photonics Center at Boston University. H.Z.G. acknowledges the support of a BUnano Cross-Disciplinary Fellowship. P.T. acknowledges the National Natural Science Foundation of China (Grant No. 11874350) and CAS Key Research Program of Frontier Sciences (Grant No. ZDBS-LY-SLH004). Some of the TEM imaging was performed at the Center for Nanoscale Systems (CNS), a member of the National Nanotechnology Coordinated Infrastructure Network (NNCI), which is supported by the National Science Foundation under NSF award no. 1541959. CNS is part of Harvard University. Work at the Molecular Foundry was supported by the Office of Science, Office of Basic Energy Sciences, of the U.S. Department of Energy under Contract No. DE-AC02-05CH11231. This material is based upon work supported by the U.S. Department of Energy, Office of Science, Office of Workforce Development for Teachers and Scientists, Office of Science Graduate Student Research (SCGSR) program. The SCGSR program is administered by the Oak Ridge Institute for Science and Education for the DOE under contract number DE-SC0014664. QM acknowledges support from the NSF Career program (award number DMR-2143426) and the CIFAR Azrieli Global Scholars program. We acknowledge Dr. X. An and Dr. B. M. Reinhard for help with SEM and EDS measurements.

Conflict of interest On behalf of all authors, the corresponding author states that there is no conflict of interest.

References

1. Y. Zhang, Y.-W. Tan, H.L. Stormer, and P. Kim, Experimental observation of the quantum Hall effect and Berry's phase in graphene. *Nature* 438, 201 (2005).
2. X. Qian, J. Liu, L. Fu, and J. Li, Quantum spin hall effect in two-dimensional transition metal dichalcogenides. *Science* 346(6215), 1344 (2005).
3. A. Splendiani, L. Sun, Y. Zhang, T. Li, J. Kim, C.-Y. Chim, G. Galli, and F. Wang, Emerging photoluminescence in monolayer MoS_2. *Nano Lett.* 10, 1271 (2010).
4. K.F. Mak, C. Lee, J. Hone, J. Shan, and T.F. Heinz, Atomically thin MoS_2: a new direct-gap semiconductor. *Phys. Rev. Lett.* 105, 136805 (2010).
5. K.S. Novoselov, D. Jiang, F. Schedin, T.J. Booth, V.V. Khotkevich, S.V. Morozov, and A.K. Geim, Two-dimensional atomic crystals. *Proc. Natl. Acad. Sci. U.S.A.* 102, 10451 (2005).
6. K.S. Novoselov, Electric field effect in atomically thin carbon films. *Science* 306, 666 (2004).
7. S. Bae, H. Kim, Y. Lee, X. Xu, J.S. Park, Y. Zheng, J. Balakrishnan, T. Lei, H.R. Kim, Y.I. Song, Y.J. Kim, K.S. Kim, B. Özyilmaz, J.H. Ahn, B.H. Hong, and S. Iijima, Roll-to-roll production of 30-inch graphene films for transparent electrodes. *Nat. Nanotechnol.* 5, 8 (2010).
8. Y. Hao, Y. Hao, M.S. Bharathi, L. Wang, Y. Liu, H. Chen, S. Nie, X. Wang, H. Chou, C. Tan, B. Fallahazad, H. Ramanarayan, C.W. Magnuson, E. Tutuc, B.I. Yakobson, K.F. McCarty, Y.W. Zhang, P. Kim, J. Hone, L. Colombo, and R.S. Ruoff, The role of surface oxygen in the growth of large single-crystal graphene on copper. *Science* 342, 720 (2013).
9. A. Nagashima, N. Tejima, Y. Gamou, T. Kawai, and C. Oshima, Electronic structure of monolayer hexagonal boron nitride physisorbed on metal surfaces. *Phys. Rev. Lett.* 75, 3918 (1995).
10. Y. Zhan, Z. Liu, S. Najmaei, P.M. Ajayan, and J. Lou, Large-area vapor-phase growth and characterization of MoS_2 atomic layers on a SiO_2 substrate. *Small* 8, 966 (2012).
11. H. Liu, M. Si, S. Najmaei, A.T. Neal, Y. Du, P.M. Ajayan, J. Lou, and P.D. Ye, Statistical study of deep submicron dual-gated field-effect transistors on monolayer chemical vapor deposition molybdenum disulfide films. *Nano Lett.* 13, 2640 (2013).
12. C.J. Carmalt, I.P. Parkin, and E.S. Peters, Atmospheric pressure chemical vapour deposition of WS_2 thin films on glass. *Polyhedron* 22, 1499 (2003).
13. M. Naguib, V.N. Mochalin, M.W. Barsoum, and Y. Gogotsi, 25th anniversary article: MXenes: a new family of two-dimensional materials. *Adv. Mater.* 26, 992 (2014).
14. J. Mannix, X.F. Zhou, B. Kiraly, J.D. Wood, D. Alducin, B.D. Myers, X. Liu, B.L. Fisher, U. Santiago, J.R. Guest, M.J. Yacaman, A. Ponce, A.R. Oganov, M.C. Hersam, and N.P. Guisinger, Synthesis of borophenes: anisotropic, two-dimensional boron polymorphs. *Science* 350, 1513 (2015).
15. Z.Y. Al Balushi, K. Wang, R.K. Ghosh, R.A. Vilá, S.M. Eichfeld, J.D. Caldwell, X.E. Qin, Y.C. Lin, P.A. DeSario, G. Stone, S. Subramanian, D.F. Paul, R.M. Wallace, S. Datta, J.M. Redwing, and J.A. Robinson, Two-dimensional gallium nitride realized via graphene encapsulation. *Nat. Mater.* 15, 1166 (2016).
16. A. Zavabeti, J.Z. Ou, B.J. Carey, N. Syed, R. Orrell-Trigg, E.L.H. Mayes, C. Xu, O. Kavehei, A.P. O'Mullane, R.B. Kaner, K. Kalantar-zadeh, and T. Daeneke, A liquid metal reaction environment for the room-temperature synthesis of atomically thin metal oxides. *Science* 358, 332 (2017).
17. N. Syed, A. Zavabeti, K.A. Messalea, E.D. Gaspera, A. Elbourne, A. Jannat, M. Mohiuddin, B.Y. Zhang, G. Zheng, L. Wang, S.P. Russo, D. Esrafilzadeh, C.F. McConville, K. Kalantar-Zadeh, and T. Daeneke, Wafer-sized ultrathin gallium and indium nitride nanosheets through the ammonolysis of liquid metal derived oxides. *J. Am. Chem. Soc.* 141, 104 (2019).
18. Y. Chen, K. Liu, J. Liu, T. Lv, B. Wei, T. Zhang, M. Zeng, Z. Wang, and L. Fu, Growth of 2D GaN single crystals on liquid metals. *J. Am. Chem. Soc.* 140, 16392 (2018).
19. J. Cao, T. Li, H. Gao, Y. Lin, X. Wang, H. Wang, T. Palacios, and X. Ling, Realization of 2D crystalline metal nitrides via selective atomic substitution. *Sci. Adv.* 6, eaax8784 (2020).
20. H.L. Zhuang, A.K. Singh, and R.G. Hennig, Computational discovery of single-layer III–V materials. *Phys. Rev. B* 87, 165415 (2013).
21. A.K. Singh and R.G. Hennig, Computational synthesis of single-layer gan on refractory materials. *Appl. Phys. Lett.* 105, 051604 (2014).
22. C.L. Freeman, F. Claeyssens, N.L. Allan, and J.H. Harding, Graphitic nanofilms as precursors to wurtzite films: theory. *Phys. Rev. Lett.* 96, 066102 (2006).
23. L.E. Brus, Electron-electron and electron-hole interactions in small semiconductor crystallites: the size dependence of the lowest excited electronic state. *J. Chem. Phys.* 80, 4403 (1984).
24. J.W. Chung, W.E. Hoke, E.M. Chumbes, and T. Palacios, AlGaN/GaN HEMT with 300-GHz f_{max}. *IEEE Electron Device Lett.* 31, 195 (2010).
25. E. Aklimi, D. Piedra, K. Tien, T. Palacios, and K.L. Shepard, Hybrid CMOS/GaN 40-MHz maximum 20-V input DC–DC multiphase buck converter. *IEEE J. Solid State Circuits* 52, 1618 (2017).
26. J.W. Chung, J. Lee, E.L. Piner, and T. Palacios, Seamless on-wafer integration of Si(100) MOSFETs and GaN HEMTs. *IEEE Electron Device Lett.* 30, 1015 (2009).
27. H.W. Then, S. Dasgupta, M. Radosavljevic, P. Agababov, I. Ban, R. Bristol, M. Chandhok, S. Chouksey, B. Holybee, C.Y. Huang, B. Krist, K. Jun, K. Lin, N. Nidhi,T. Michaelos, B. Mueller, R. Paul, J. Peck, W. Rachmady, D. Staines, T. Talukdar, N. Thomas, T. Tronic, P. Fischer, W. Hafez, 3D heterogeneous integration of high performance high-K Metal gate GaN NMOS and Si PMOS transistors on 300mm high-resistivity si substrate for energy-efficient and compact power delivery, RF (5G and beyond) and SoC applications, in *2019 IEEE International Electron Devices Meeting (IEDM)* (2019), pp. 17.3.1–17.3.4.
28. N. Sanders, D. Bayerl, G. Shi, K.A. Mengle, and E. Kioupakis, Electronic and optical properties of two-dimensional GaN from first-principles. *Nano Lett.* 17, 7345 (2017).
29. T. Lei, M. Fanciulli, R.J. Molnar, T.D. Moustakas, R.J. Graham, and J. Scanlon, Epitaxial growth of zinc blende and wurtzitic gallium nitride thin films on (001) silicon. *Appl. Phys. Lett.* 59, 944 (1991).
30. D. Doppalapudi, E. Iliopoulos, S.N. Basu, and T.D. Moustakas, Epitaxial growth of gallium nitride thin films on A-plane sapphire by molecular beam epitaxy. *J. Appl. Phys.* 85, 3582 (1999).
31. S.M. Islam, K. Lee, J. Verma, V. Protasenko, S. Rouvimov, S. Bharadwaj, H.G. Xing, and D. Jena, MBE-grown 232–270 Nm deep-UV LEDs using monolayer thin binary GaN/AlN quantum heterostructures. *Appl. Phys. Lett.* 110, 041108 (2017).
32. R. Yan, G. Khalsa, S. Vishwanath, Y. Han, J. Wright, S. Rouvimov, D.S. Katzer, N. Nepal, B.P. Downey, D.A. Muller, H.G. Xing, D.J. Meyer, and D. Jena, GaN/NbN epitaxial semiconductor/superconductor heterostructures. *Nature* 555, 183 (2018).
33. S.J. Rosner, E.C. Carr, M.J. Ludowise, G. Girolami, and H.I. Erikson, Correlation of cathodoluminescence inhomogeneity with microstructural defects in epitaxial GaN grown by metalorganic chemical-vapor deposition. *Appl. Phys. Lett.* 70, 420 (1997).
34. H. Yoo, K. Chung, Y.S. Choi, C.S. Kang, K.H. Oh, M. Kim, and G.-C. Yi, Microstructures of GaN thin films grown on graphene layers. *Adv. Mater.* 24, 515 (2012).

35. L. Liu and J.H. Edgar, Substrates for gallium nitride epitaxy. *Mater. Sci. Eng. R Rep.* 37, 61 (2002).
36. G. Lian, The pros and cons of GaN family of materials compared with other alternatives regarding optoelectronic applications, in *2020 7th International Forum on Electrical Engineering and Automation (IFEEA)* (2020), pp. 149–152.
37. I.V. Zabrosaev, M.G. Kozodaev, R.I. Romanov, A.G. Chernikova, P. Mishra, N.V. Doroshina, A.V. Arsenin, V.S. Volkov, A.A. Koroleva, and A.M. Markeev, Field-effect transistor based on 2D microcrystalline MoS_2 film grown by sulfurization of atomically layer deposited MoO_3. *Nanomaterials* 12, 19 (2022).
38. Q.H. Wang, K. Kalantar-Zadeh, A. Kis, J.N. Coleman, and M.S. Strano, Electronics and optoelectronics of two-dimensional transition metal dichalcogenides. *Nat. Nanotechnol.* 7, 699 (2012).
39. M. Vinet, P. Batude, C. Fenouillet-Beranger, F. Clermidy, L. Brunet, O. Rozeau, J. M Hartmannn, O. Billoint, G. Cibrario , B. Previtali, C. Tabone, B. Sklenard, O. Turkyilmaz, F. Ponthenier, N. Rambal, M.P. Samson, F. Deprat, V. Lu, L. Pasini, S. Thuries, H. Sarhan, J.E. Michallet, O. Faynot, Monolithic 3D integration: A powerful alternative to classical 2D scaling, in *2014 SOI-3D-Subthreshold Microelectronics Technology Unified Conference (S3S)* (2014), pp. 1–3.
40. M.M. Shulaker, T.F. Wu, M.M. Sabry, H. Wei, H.S.P. Wong, S. Mitra, Monolithic 3D integration: a path from concept to reality, in *2015 Design, Automation Test in Europe Conference Exhibition (DATE)* (2015), pp. 1197–1202.
41. D. Ruzmetov, K. Zhang, G. Stan, B. Kalanyan, G.R. Bhimanapati, S.M. Eichfeld, R.A. Burke, P.B. Shah, T.P. O'Regan, F.J. Crowne, A.G. Birdwell, J.A. Robinson, A.V. Davydov, and T.G. Ivanov, Vertical 2D/3D semiconductor heterostructures based on epitaxial molybdenum disulfide and gallium nitride. *ACS Nano* 10, 3580 (2016).
42. J. Jiang, K. Parto, W. Cao, and K. Banerjee, Ultimate monolithic-3D integration with 2D materials: rationale, prospects, and challenges. *IEEE J. Electron Devices Soc.* 7, 878 (2019).
43. S.-H. Bae, H. Kum, W. Kong, Y. Kim, C. Choi, B. Lee, P. Lin, Y. Park, and J. Kim, Integration of bulk materials with two-dimensional materials for physical coupling and applications. *Nat. Mater.* 18, 6 (2019).
44. X. Wang, Y. Sheng, R.J. Chang, J.K. Lee, Y. Zhou, S. Li, T. Chen, H. Huang, B.F. Porter, H. Bhaskaran, and J.H. Warner, Chemical vapor deposition growth of two-dimensional monolayer gallium sulfide crystals using hydrogen reduction of Ga_2S_3. *ACS Omega* 3, 7897 (2018).
45. P. Hu, L. Wang, M. Yoon, J. Zhang, W. Feng, X. Wang, Z. Wen, J.C. Idrobo, Y. Miyamoto, D.B. Geohegan, and K. Xiao, Highly responsive ultrathin GaS nanosheet photodetectors on rigid and flexible substrates. *Nano Lett.* 13, 1649 (2013).
46. M. Kumar, M.K. Rajpalke, B. Roul, T.N. Bhat, P. Misra, L.M. Kukreja, N. Sinha, A.T. Kalghatgi, and S.B. Krupanidhi, Temperature-dependent photoluminescence of GaN grown on β-Si_3N_4/Si (111) by plasma-assisted MBE. *J. Lumin.* 131, 614 (2011).
47. E.J. Tarsa, B. Heying, X.H. Wu, P. Fini, S.P. DenBaars, and J.S. Speck, Homoepitaxial growth of GaN under Ga-stable and N-stable conditions by plasma-assisted molecular beam epitaxy. *J. Appl. Phys.* 82, 5472 (1997).
48. V.-T. Rangel-Kuoppa, C.G. Aguilar, and V. Sánchez-Reséndiz, Structural, optical and electrical study of undoped GaN layers obtained by metalorganic chemical vapor deposition on sapphire substrates. *Thin Solid Films* 519, 2255 (2011).
49. S. Hu, S. Liu, Z. Zhang, H. Yan, Z. Gan, and H. Fang, A novel MOCVD reactor for growth of high-quality GaN-related LED layers. *J. Cryst. Growth* 415, 72 (2015).
50. Y. Zhang, Z. Chen, W. Li, A.R. Arehart, S.A. Ringel, and H. Zhao, Metalorganic chemical vapor deposition gallium nitride with fast growth rate for vertical power device applications. *Phys. Status Solidi (A)* 218, 2000469 (2021).
51. L.T. Romano, J.E. Northrup, and M.A. O'Keefe, Inversion domains in GaN grown on sapphire. *Appl. Phys. Lett.* 69, 2394 (1996).
52. R. Delgado Carrascon, S. Richter, M. Nawaz, P.P. Paskov, and V. Darakchieva, Hot-wall MOCVD for high-quality homoepitaxy of GaN: understanding nucleation and design of growth strategies. *Cryst. Growth Des.* 22, 7021 (2022).
53. N.R. Glavin, K.D. Chabak, E.R. Heller, E.A. Moore, T.A. Prusnick, B. Maruyama, D.E. Walker Jr., D.L. Dorsey, Q. Paduano, and M. Snure, Flexible gallium nitride for high-performance, strainable radio-frequency devices. *Adv. Mater.* 29, 1701838 (2017).
54. A.M. Berhane, K.Y. Jeong, Z. Bodrog, S. Fiedler, T. Schröder, N.V. Triviño, T. Palacios, A. Gali, M. Toth, D. Englund, and I. Aharonovich, Bright room-temperature single-photon emission from defects in gallium nitride. *Adv. Mater.* 29, 1605092 (2017).
55. T. Honda, Y. Inao, K. Konno, K. Mineo, S. Kumabe, and H. Kawanishi, Deposition of amorphous GaN by compound source molecular beam epitaxy for electroluminescent devices. *Phys. Status Solidi (A)* 192, 461 (2002).
56. C. Liu, Y.K. Ooi, S.M. Islam, H.G. Xing, D. Jena, and J. Zhang, 234 Nm and 246 Nm AlN-Delta-GaN quantum well deep ultraviolet light-emitting diodes. *Appl. Phys. Lett.* 112, 011101 (2018).
57. C. Liu, Y.K. Ooi, S.M. Islam, J. Verma, H.G. Xing, D. Jena, and J. Zhang, Physics and polarization characteristics of 298 Nm AlN-Delta-GaN quantum well ultraviolet light-emitting diodes. *Appl. Phys. Lett.* 110, 071103 (2017).
58. S.M. Islam, V. Protasenko, S. Rouvimov, H.G. Xing, and D. Jena, Sub-230 Nm deep-UV emission from GaN quantum disks in AlN grown by a modified Stranski–Krastanov mode. *Jpn. J. Appl. Phys.* 55, 05FF06 (2016).
59. G. Santana, O. De Melo, J. Aguilar-Hernández, R. Mendoza-Pérez, B.M. Monroy, A. Escamilla-Esquivel, M. López-López, F. De Moure, L.A. Hernández, and G. Contreras-Puente, Photoluminescence study of gallium nitride thin films obtained by infrared close space vapor transport. *Materials* 6, 1050 (2013).
60. H. Amano, Growth of GaN layers on sapphire by low-temperature-deposited buffer layers and realization of p-type GaN by magesium doping and electron beam irradiation (Nobel Lecture). *Angew. Chem. Int. Ed.* 54, 7764 (2015).
61. P. Chen, R. Zhang, Z.M. Zhao, D.J. Xi, B. Shen, Z.Z. Chen, Y.G. Zhou, S.Y. Xie, W.F. Lu, and Y.D. Zheng, Growth of high quality GaN layers with AlN buffer on Si(111) substrates. *J. Cryst. Growth* 225, 150 (2001).
62. Y. Feng, X. Yang, Z. Zhang, D. Kang, J. Zhang, K. Liu, X. Li, J. Shen, F. Liu, T. Wang, P. Ji, F. Xu, N. Tang, T. Yu, X. Wang, D. Yu, W. Ge, and B. Shen, GaN-on-Si(100): epitaxy of single-crystalline GaN film on CMOS-compatible Si(100) substrate buffered by graphene. *Adv. Funct. Mater.* 29, 1970293 (2019).
63. Z. Qin, G. Qin, X. Zuo, Z. Xiong, and M. Hu, Orbitally driven low thermal conductivity of monolayer gallium nitride (GaN) with planar honeycomb structure: a comparative study. *Nanoscale* 9, 4295 (2017).
64. Y. Zheng, X. Tang, W. Wang, L. Jin, and G. Li, Large-size ultrathin α-Ga_2S_3 nanosheets toward high-performance photodetection. *Adv. Funct. Mater.* 31, 2008307 (2021).
65. K. Eriguchi, C. Biaou, S. Das, K.M. Yu, J. Wu, and O.D. Dubon, Temperature-dependent growth of hexagonal and monoclinic gallium sulfide films by pulsed-laser deposition. *AIP Adv.* 10, 105215 (2020).
66. M. Grodzicki, J.-G. Rousset, P. Ciechanowicz, E. Piskorska-Hommel, and D. Hommel, XPS studies on the role of arsenic incorporated into GaN. *Vacuum* 167, 73 (2019).

67. D.M. Hofmann, B.K. Meyer, H. Alves, F. Leiter, W. Burkhard, N. Romanov, Y. Kim, J. Krüger, and E.R. Weber, The red (1.8 EV) luminescence in epitaxially grown GaN. *Phys. Status Solidi (A)* 180, 261 (2000).
68. Y. Yu, Y. Yu, Y. Cai, W. Li, A. Gurarslan, H. Peelaers, D.E. Aspnes, C.G. Van de Walle, N.V. Nguyen, Y.W. Zhang, and L. Cao, Exciton-dominated dielectric function of atomically thin MoS_2 films. *Sci. Rep.* 5, 1 (2015).
69. G.Y. Jia, Y. Liu, J.Y. Gong, D.Y. Lei, D.L. Wang, and Z.X. Huang, Excitonic quantum confinement modified optical conductivity of monolayer and few-layered MoS_2. *J. Mater. Chem. C* 4, 8822 (2016).
70. H. Morkoç, S. Strite, G.B. Gao, M.E. Lin, B. Sverdlov, and M. Burns, Large-band-gap SiC, III-V nitride, and II-VI ZnSe-based semiconductor device technologies. *J. Appl. Phys.* 76, 1363 (1994).
71. L. Mallet-Dida, P. Disseix, F. Réveret, F. Médard, B. Alloing, J. Zúñiga-Pérez, and J. Leymarie, The Low temperature limit of the excitonic mott density in GaN: an experimental reassessment. *New J. Phys.* 24, 033031 (2022).
72. D.K. Lewis and S. Sharifzadeh, Defect-induced exciton localization in bulk gallium nitride from many-body perturbation theory. *Phys. Rev. Mater.* 3, 114601 (2019).
73. M.T. Hibberd, V. Frey, B.F. Spencer, P.W. Mitchell, P. Dawson, M.J. Kappers, R.A. Oliver, C.J. Humphreys, and D.M. Graham, Dielectric response of wurtzite gallium nitride in the terahertz frequency range. *Solid State Commun.* 247, 68 (2016).